FERMILAB-PUB-15-510-A

The Astrophysical Journal, 833:162 (7pp), 2016 December 20 doi:10.3847/1538-4357/833/2/162
© 2016. The American Astronomical Society. All rights reserved.

THE EFFECTS OF DARK MATTER ANNIHILATION ON COSMIC REIONIZATION

Alexander A. Kaurov[1], Dan Hooper[1,2,3], and Nickolay Y. Gnedin[1,2,3]
[1] Department of Astronomy & Astrophysics, The University of Chicago, Chicago, IL 60637 USA; kaurov@uchicago.edu
[2] Particle Astrophysics Center, Fermi National Accelerator Laboratory, Batavia, IL 60510, USA
[3] Kavli Institute for Cosmological Physics and Enrico Fermi Institute, The University of Chicago, Chicago, IL 60637, USA
Received 2015 December 2; revised 2016 October 21; accepted 2016 October 21; published 2016 December 15

ABSTRACT

We revisit the possibility of constraining the properties of dark matter (DM) by studying the epoch of cosmic reionization. Previous studies have shown that DM annihilation was unlikely to have provided a large fraction of the photons which ionized the universe, but instead played a subdominant role relative to stars and quasars. The DM might, however, have begun to efficiently annihilate with the formation of primordial microhalos at $z \sim 100$–200, much earlier than the formation of the first stars. Therefore, if DM annihilation ionized the universe at even the percent level over the interval $z \sim 20$–100, it could leave a significant imprint on the global optical depth, τ. Moreover, we show that cosmic microwave background polarization data and future 21 cm measurements will enable us to more directly probe the DM contribution to the optical depth. In order to compute the annihilation rate throughout the epoch of reionization, we adopt the latest results from structure formation studies and explore the impact of various free parameters on our results. We show that future measurements could make it possible to place constraints on the DM's annihilation cross-sections, which are at a level comparable to those obtained from the observations of dwarf galaxies, cosmic-ray measurements, and studies of recombination.

Key words: cosmology: theory – dark ages, reionization, first stars – dark matter

1. INTRODUCTION

Despite recent advances in the observations of the high-redshift universe, the physics of cosmic reionization remains uncertain. Current observations of the Lyα forest (Becker et al. 2015) allow us to probe the final stages of reionization, and cosmic microwave background (CMB) polarization data can be used to place very broad constraints on its duration (Zahn et al. 2012). Upcoming experiments, such as the *James Webb Space Telescope* (*JWST*), and the introduction of 21 cm cosmology, will make it possible to observe the high-redshift universe in much greater detail and to place much stricter constraints on the processes responsible for the reionization of the universe.

The main objective pertaining to cosmic reionization is to determine the sources of the ionizing photons. The most widely discussed sources for hydrogen reionization are the stars within galaxies, while quasars are often thought to be primarily responsible for reionizing helium. Recent observations (Madau & Haardt 2015) argue in favor of quasar activity during hydrogen reionization as well. Other sources have also been proposed; for example, X-ray binaries (Fialkov et al. 2014).

Within this context, the annihilation of dark matter (DM) particles is an interesting process. The products of DM annihilation can affect the intergalactic medium (IGM), and, therefore, change the global ionization and thermal histories of our universe. In contrast to some previous studies (Belikov & Hooper 2009b; Cirelli et al. 2009), we do not imagine that the DM is the only, or even the primary, source of ionizing photons (see also, Furlanetto et al. 2006; Mapelli et al. 2006; Ripamonti et al. 2007a, 2007b; Shchekinov & Vasiliev 2007; Valdés et al. 2007; Chuzhoy 2008; Hütsi et al. 2009; Natarajan & Schwarz 2009; Cumberbatch et al. 2010). We instead expect that the DM played a relatively minor role in cosmic reionization. In this paper, we consider only the models of DM with minimal halo mass lower than $10^{-6} M_{\odot}$ (Profumo et al. 2006), which start to form at $z \sim 100$–200 (Diemand et al. 2005; Ishiyama 2014; Angulo et al. 2016). This is in contrast to the stars, which begin to form at $z \sim 15$–20. If DM ionized the universe to the level of a few percent over the redshift interval between $\sim$20–200, this would significantly impact the global optical depth, τ. We will show that the constraints on τ from the combination of future CMB and 21 cm observations will provide a powerful tool for constraining the properties of particle DM.

The remainder of this paper is structured as followed. First, in Section 2, we evaluate the total rate of DM annihilation, including the boost factor, which quantifies the amount of structure over cosmic history. In Section 3, we discuss the interactions between the DM annihilation products and the IGM. Finally, we present in Section 4 current and projected constraints on the DM annihilation cross-section. We summarize these constraints and discuss the prospects for further developments in Section 5.

2. BOOST FACTOR

The global rate of DM annihilation at a given redshift is proportional to $\langle n_{\rm DM}^2 \rangle$, where $n_{\rm DM}$ is the number density of DM particles. As a result of inhomogeneities in the DM density, the annihilation rate is enhanced by the following "boost factor":

$$B = \frac{\langle n_{\rm DM}^2 \rangle}{\langle n_{\rm DM} \rangle^2}. \quad (1)$$

In order to calculate the boost factor properly, one needs to integrate over the relevant volume, and over all scales. Unfortunately, simulations of large-scale structure do not have the resolution required to characterize such structure on very small scales. Therefore, as in other studies (Belikov & Hooper 2009a; Cirelli et al. 2009; Hütsi et al. 2009; Lopez-Honorez et al. 2013; Poulin et al. 2015; Liu et al. 2016a), we must rely on extrapolations of the halo mass function and the relationship between halo mass and concentration.

Table 1
Free Parameters and Their Adopted Values

Parameter Description	Low	Medium	High
Section 2.1 Mass function cutoff (in $\log_{10} M_\odot$)	−6	−9	−12
Section 2.2 Modified Navarro–Frenk–White (NFW) profile for small halos	No	Yes	Yes
Section 2.3 Scatter of concentrations (in $\sigma_{\log_{10} c}$)	0.08	0.16	0.24
Section 2.4 Subhalo mass function	No	Yes	Yes
Section 2.5 Caustics and nonspherical profiles	None	None	2.0

We attempt to approach this problem systematically, by parameterizing the uncertainties regarding the distribution of DM and then classifying the possible values for the parameters into three categories, which we label as *Low*, *Medium*, and *High* (see Table 1). When we consider this full range of parameters, the boost factors calculated during reionization span approximately two orders of magnitude; see Figure 1. In the following subsections, we will discuss each of these individual parameters and their impact on the DM annihilation rate.

2.1. Halo Mass Function

Halo mass function models can be based on analytic calculations, or fitted to the results of numerical simulations. Most models based on numerical simulations (for example, Tinker et al. 2008 and their extension to higher redshifts by Behroozi et al. 2013) are tuned to match the characteristics of large halos, $10^8 M_\odot < M < 10^{15} M_\odot$. Lower-mass halos, in which we are particularly interested, can also be explored numerically, but require dedicated simulations, such as those carried out by Diemand et al. (2005). Studies such as these find a behavior of $dN/dM \propto M^{-2}$, which can be modeled with a simple Press–Schechter mass function (Press & Schechter 1974). Although there are known deviations from the Press–Schechter halo mass function, these are important only at redshifts below ∼20 and for masses above $\sim 10^6$–$10^8 M_\odot$. In our calculations, we neglect halos more massive than $10^6 M_\odot$, for which the baryonic content increases the rate of atomic processes, which affect the local IGM, effectively reducing the contribution to global reionization (Kaurov 2016); this choice has little impact on our results.

The halo mass function is further predicted to be truncated below a minimum mass, $M_{\rm min}$, which is determined by the temperature at which the DM became kinetically decoupled. Although predictions for $M_{\rm min}$ depend on the specific interactions between the DM and the Standard Model, and are thus highly model dependent, most models of DM as weakly interacting massive particles feature values in the range of 10^{-3}–$10^{-12} M_\odot$ (Green et al. 2004; Profumo et al. 2006). The halos of such low masses start to form very early, causing the boost factor to start to rapidly grow at $z \sim 100$.

In Figure 1, we plot the range of boost factors found when allowing $M_{\rm min}$ to vary between 10^{-6}–$10^{-12} M_\odot$ (black, vertically hatched), and when fixed to $10^{-9} M_\odot$ (red, diagonally hatched). The minimum mass is the second most important parameter we have considered, after the inner slope of the halo profile, which we discuss in the next subsection.

In Section 4, we show that the constraining power of the optical depth for the model with $M_{\rm min} = 10^{-6} M_\odot$ is already very weak compared to the constraints from recombination.

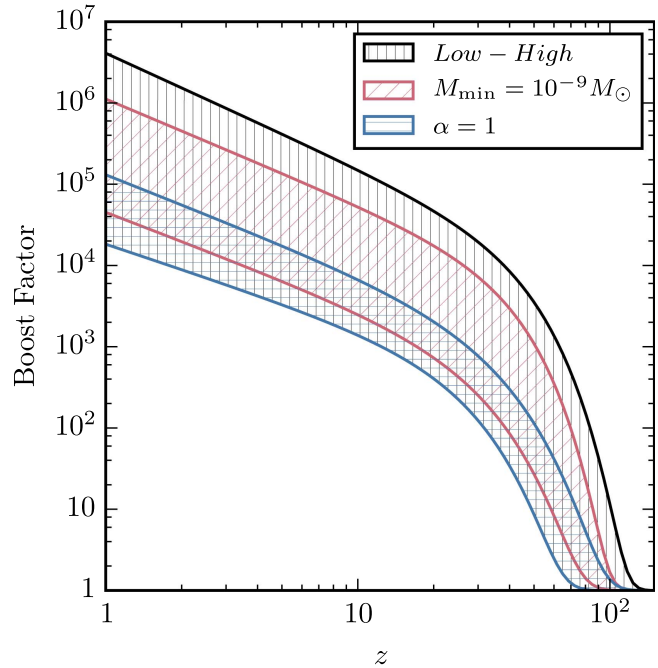

Figure 1. Range of boost factors evaluated using the *Low* and *High* parameters listed in Table 1. The black and vertically hatched region spans the entire range of these parameters. The red and diagonally hatched region is the same, but with $M_{\rm min}$ fixed to $10^{-9} M_\odot$. The blue and horizontally hatched region has the value of the inner slope, α, fixed to unity.

That is why, in this study, we adopt $10^{-6} M_\odot$ as the highest value of $M_{\rm min}$.

2.2. Halo Profiles

Beginning with the *Low* case, we adopt the standard NFW radial profile for DM halos (Navarro et al. 1997). Other types of commonly adopted profiles (e.g., Einasto) do not significantly modify our results, as most of the DM annihilation takes place around the scale radius, where such profiles are very similar. An exception, however, can be found for profiles with much steeper inner slopes. It is common to generalize the NFW profile such that its inner slope, α, is treated as a free parameter:

$$\rho(r) = \frac{\rho_0}{(r/r_S)^\alpha (1 + r/r_S)^{(3-\alpha)}}. \quad (2)$$

For the standard NFW case, $\alpha \equiv 1$. For the *Medium* and *High* cases, we adopt the fit for α provided by Ishiyama (2014)

$$\alpha = -0.123 \log(M_{\rm vir}/M_{\rm min}) + 1.461, \quad (3)$$

where $M_{\rm vir}$ is the virial mass of a halo and $M_{\rm min}$ is the minimum halo mass. For masses, which yield a value less than unity, we adopt $\alpha = 1$. This parameterization significantly increases the annihilation rate in the smallest halos relative to the standard NFW prescription.

In Figure 1, we show the boost factor calculated in the *Low* and *High* cases, with α fixed to unity (blue, horizontally hatched). This illustrates that the inner profile of the smallest mass halos can significantly impact the global boost factor. We note that although such steep profiles for the smallest halos are supported by simulations (Ishiyama 2014), it is not yet clear whether this behavior has been reliably resolved, and will require further studies to confirm.

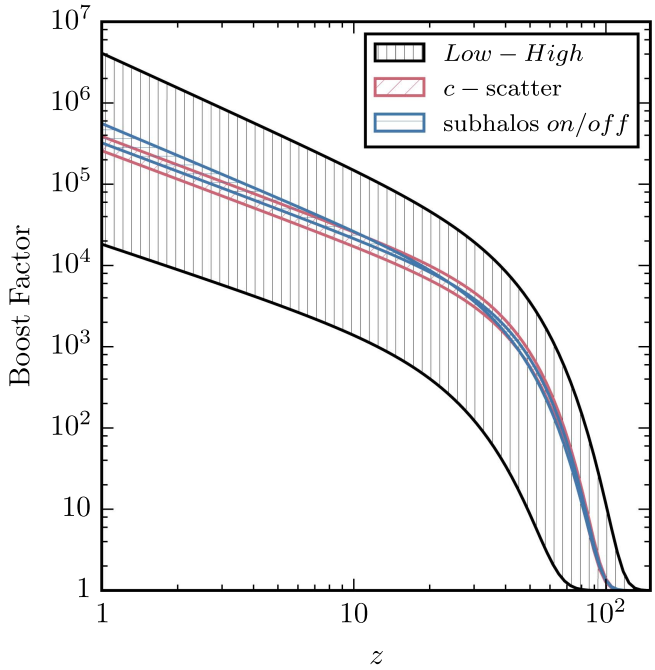

Figure 2. Range of boost factors associated with variations in the distribution of halo concentrations (red, diagonally hatched) and with variations in the treatment of subhalos (blue, horizontally hatched), while keeping all other parameters fixed to their *Medium* values (see Table 1). The black hatched region denotes the full range of boost factors between the *Low* and *High* parameter sets.

2.3. Halo Concentrations

For the concentrations of our DM halos, we adopt the model of Diemer & Kravtsov (2015). Again, since this model is based on simulations, only halos with masses greater than $\sim 10^{10}\,M_\odot$ are directly probed. However, given that these concentrations are in fairly good agreement with those from simulations of high-redshift ($z \sim 30$) microhalos (see Figure 8 of Diemer & Kravtsov 2015), we are optimistic about the reliability of this application.

Even though the average concentration for a halo of a given mass is well defined, there is a significant degree of halo-to-halo variation in this quantity. In Diemer & Kravtsov (2015), the authors report that the 68% rms scatter in $\log_{10} c_{200c}$ is $\sim$0.16 around the median value. Depending on the underlying distribution, such variations can increase the boost factor by 15%–50%. We adopt the probability distribution function for concentrations as described in Moline et al. (2015). For our *Low*, *Medium,* and *High* scenarios, we adopt values of $\sigma_{\log_{10} c} = 0.08$, 0.16, and 0.24, respectively. The impact of this variation is small compared to other parameters considered in this study (see Figure 2).

2.4. Subhalos

The halo mass function, adopted in this study, does not account for the subhalos which reside within larger halos. The presence of such subhalos is predicted to enhance the DM annihilation rate. To estimate their impact, we followed the approach of Sanchez-Conde & Prada (2014), finding that the presence of subhalos does not increase the global boost factor by a large factor (see Figure 2). More specifically, while subhalos can play a significant role in the largest halos (e.g., Zavala & Afshordi 2016), such very massive halos are rare, especially at $z > 10$. For small halos at high redshifts, the impact of subhalos is insignificant due to the flattening of the concentration function at low masses. Since the presence of subhalos does not strongly impact our results, we do not explore additional effects, such as the dependence of the subhalo mass function on the concentration of the host halo (Emberson et al. 2015; Mao et al. 2015).

2.5. Nonspherical Halos

Thus far, in this study, we have assumed that DM halos and subhalos are spherically symmetric. Departures from sphericity can, however, be present during the active collapse of the first halos and during the subsequent mergers of halos. This can increase the boost factor; for example, Anderhalden & Diemand (2013) found that departures from sphericity enhance in the annihilation rate by a factor of $\sim$1.5 at $z \sim 30$ for primordial microhalos, and by an additional factor of $\sim$1.5 due to caustics. Motivated by these results, we double the total boost factor in our *High* model.

3. COSMIC IONIZATION BY DM ANNIHILATION

3.1. Efficiency of DM Annihilation in Ionizing the IGM

The annihilation of DM is characterized by the mass of the DM particle, the annihilation cross-section, $\langle \sigma v \rangle$, and the products of those annihilations. The effects of DM annihilation on the IGM depend strongly on the species and energies of the particles which are created in this process. We use the results of Cirelli et al. (2011) and Ciafaloni et al. (2011) to account for the hadronization and cascades of the DM annihilation products.[4]

In order to properly evaluate the fraction of energy produced by the annihilation which goes to the ionization of the IGM, we developed a code, which is described in detail in Kaurov (2016). The code allows us to propagate an energetic charged particles and photons on cosmological timescales and calculate the fractions of energies going into different channels such as the Inverse Compton scattering on the CMB photons and the atomic processes. In contrast to many previous studies (Shull 1979; Shull & van Steenberg 1985; Dalgarno et al. 1999; Furlanetto & Stoever 2010; Valdés et al. 2010; Dvorkin et al. 2013; Slatyer 2016), in Kaurov (2016) we consider regions with baryon overdensities, i.e., halos, and show that the energy distribution between channels is different in those regions. In particular, it was shown that overdensities in baryons effectively reduce the production of energetic photons and increase the rate of atomic processes, which affect the IGM only locally. Therefore, the halos containing baryons are generally only able to ionize themselves.

We roughly estimate that the transition between halos with and without baryons occurs around $\sim 10^6\,M_\odot$, as defined by the filtering mass (Naoz et al. 2013). The contribution to reionization from DM annihilation in larger halos is expected to be suppressed. We also note that once halos with baryons begin to appear, star formation begins and quickly overtakes DM annihilation as a source of ionizing photons.

In this study, we assume that the ionizing flux is uniform in the universe for two main reasons. First, the major contribution to the ionization flux comes from the small halos which are very common; and second, the energetic photons have low

[4] http://www.marcocirelli.net/PPPC4DMID.html

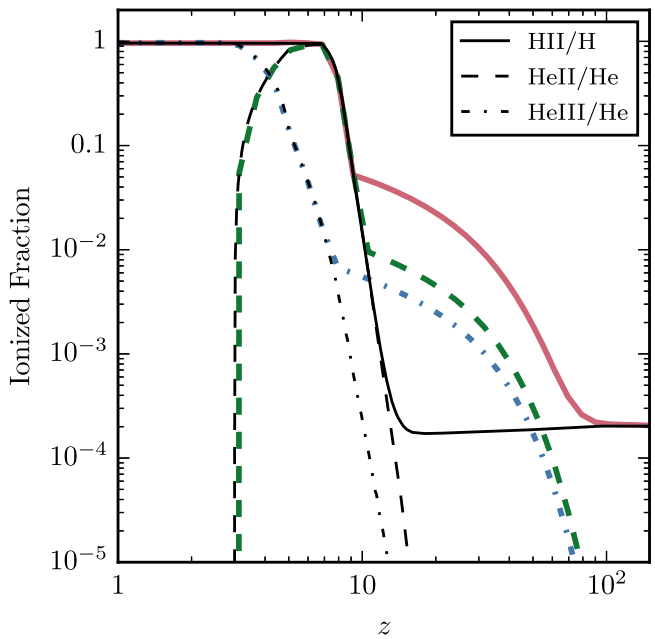

Figure 3. Fraction of ionized hydrogen (solid), helium II (dashed) and helium III (dotted–dashed) as a function of redshift in our fiducial model. The colored lines include the contribution from a 40 GeV DM particle, which annihilates to $b\bar{b}$ with a cross-section of $\sigma v = 10^{-26}\,\mathrm{cm}^3\,\mathrm{s}^{-1}$, adopting the *High* boost factor model (see Table 1). In this particular case, the effects of DM annihilation increase the optical depth, τ, from 0.059 to 0.068.

ionizing cross-section and long mean free paths compared to the distance between halos. Therefore, instead of running a full radiative transfer simulation, we assume a uniform ionization scenario up to the moment when stars start to form. We use the code from Kaurov (2016) to calculate the ionization rate per annihilation, and converge it with the boost factor evaluated in Section 2.

In realistic models (those not ruled out by other indirect detection probes), DM annihilation can ionize the universe to the level of a few percent or less before stars begin to form. Therefore, we can safely assume that the propagation of ionization fronts is not strongly affected by this small uniform ionized fraction.

In Figure 3, we plot our fiducial reionization model, which was derived from one of the numerical simulations and completed as part of the Cosmic Reionization on Computers project (Gnedin 2014; Gnedin & Kaurov 2014). The optical depth of this fiducial model is $\tau = 0.059$, compared to the value of $\tau = 0.066 \pm 0.016$ derived from polarization and temperature measurements by the Planck Collaboration et al. (2016).

3.2. Ionization Equilibrium during the Dark Ages

In order to estimate the global ionization fraction during the dark ages, we assume spatially uniform ionization by DM annihilation. Even though the large boost factors indicate that most of the DM annihilation takes place within halos, these halos are distributed relatively uniformly due to the flat bias function at low masses. Furthermore, the radiation produced through DM annihilation typically has a long mean free path, exceeding the average distance between primordial halos.

The process of ionization competes with the recombination of ionized particles with electrons. The global recombination rate of hydrogen is given by (a similar equation can be written for helium ions)

$$R = C\bar{n}_{\mathrm{H\,II}}\bar{n}_e\alpha_H, \tag{4}$$

where α_H is a recombination coefficient, $\bar{n}_{\mathrm{H\,II}}$ and $\bar{n}_e$ are number densities of protons and electrons, and C is the clumping factor, which characterizes the substructure of baryons (analogous to the boost factor for DM annihilation). At high redshifts, when little baryonic structure exists, the clumping factor is of order unity.

From the rate of ionization and recombination at each redshift, we can calculate the abundance of each ion. Although the small ionized fraction should affect the propagation of ionization fronts created by galaxies, we neglect this affect and assume that our fiducial reionization model is not altered dramatically below redshift $\sim$10 (as is supported, for example, in Figure 3).

4. RESULTS

For a given particle DM model and model for the redshift-dependent boost factor, we can calculate the effects of DM annihilation on the IGM and determine the evolution of the universe's ionization fraction. We show such an example in Figure 3, for the representative example of a 40 GeV DM particle, which annihilates to $b\bar{b}$ with a cross-section of $\sigma v = 10^{-26}\,\mathrm{cm}^3\,\mathrm{s}^{-1}$, adopting the *High* boost factor model. In this model, the ionization fraction at $z \sim 10$–50 increases to the level of a few percent. As a result, the total optical depth is enhanced significantly, from 0.059 to 0.068. This illustrates that precision measurements of τ could potentially enable us to place interesting constraints on the properties of the DM.

Polarization measurements by Planck (Planck Collaboration et al. 2016) using the Low Frequency Instrument at large angular scales, combined with Planck temperature and lensing data, yield a total reionization optical depth of $\tau = 0.066 \pm 0.016$. If these measurements are combined with those of baryon acoustic oscillations, Type Ia supernovae, and the local Hubble constant (see Table 4 of Planck Collaboration 2015), the error on this quantity is further reduced to $\Delta\tau = 0.012$. Upcoming 21 cm measurements will be a very powerful tool for further constraining the contribution to the optical depth from stars (Liu et al. 2016b), and is expected to enable us to reduce the uncertainty on this parameter to the level of $\Delta\tau \sim 0.001$.

In Figure 4, we plot our constraints on the DM annihilation cross-section, for the current measurement uncertainty of $\Delta\tau = 0.012$ (red, vertically hatched), and for a future measurement with $\Delta\tau = 0.001$ (blue, horizontally hatched). Each of these results is shown as a band, which covers the range of boost factor models from *Low* to *High*, as described earlier in this paper. These results are compared to the constraints derived from observations of dwarf spheroidal galaxies by the *Fermi Gamma-Ray Space Telescope* (Fermi-LAT Collaboration 2015), measurements of the cosmic-ray positron spectrum by AMS-02 (Bergström et al. 2013), and from the impact of DM annihilation on recombination (Slatyer et al. 2009; Planck Collaboration et al. 2016). For high-mass DM particles, our constraints are less competitive with those from other observations, as high-energy electrons and photons do not interact significantly with the IGM and thus lead to very inefficient reionization.

From Figure 4, we can conclude that the constraints derived with the *Low* model are not competitive with the existing

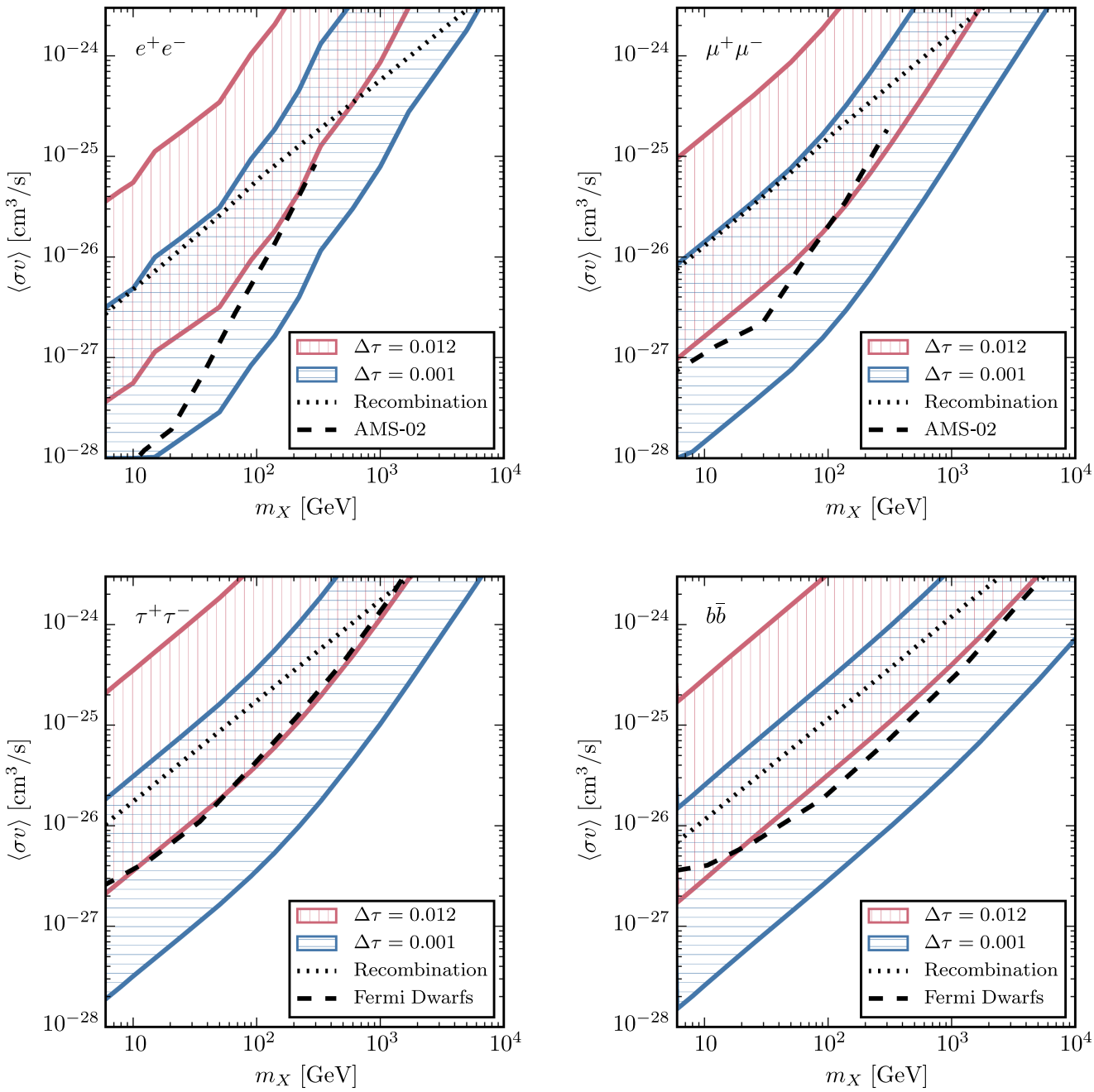

Figure 4. Constraints on the DM annihilation cross-section for e^+e^-, $\mu^+\mu^-$, $\tau^+\tau^-$ and $b\bar{b}$ final states. The red vertically hatched regions represent the constraints from current measurements, corresponding to $\Delta\tau = 0.012$, while the blue horizontally hatched regions are the constraints projected from future 21 cm measurements with $\Delta\tau = 0.001$. The width of these regions reflect the range of *Low* to *High* boost factor models (see Table 1). For comparison, we show the constraints from the impact of DM annihilation on recombination (Slatyer et al. 2009; Planck Collaboration et al. 2016) (dotted), as well as from gamma-ray observations of dwarf galaxies (Fermi-LAT Collaboration 2015) and measurements of the cosmic-ray positron spectrum (Bergström et al. 2013) (dashed).

constraints, even if the uncertainty of the optical depth is reduced to the level of 0.001. Therefore, it is safe to say that if the minimal halo mass is higher $\sim 10^{-6}\,M_\odot$, then even the most precise measurements of τ would not be able to provide any new information about the DM.

Our fiducial reionization model (without annihilating DM) was chosen to have the optical depth slightly lower than the mean measured value, therefore, leaving some room for the optical depth generated by the DM annihilation. It was chosen this way in order to have relatively conservative predictions. If one adopts another fiducial model, which has the optical depth closer to the allowed upper limit, then the constraints on the DM annihilation can be greatly improved. However, given current uncertainties in many aspects of star formation at high redshifts, we are not in a position to assume such models as fiducial. Ultimately, one has to simultaneously constrain both contributions—astrophysical (stars and quasars) and DM annihilation, but this is beyond the scope of this paper.

The global optical depth, τ, receives contributions from stars, quasars, and (possibly) annihilating DM. For the reasons mentioned above, even with a very high-precision measurement of τ, it may still be challenging to distinguish between these contributions. Fortunately, the global optical depth is not the only relevant information contained in the CMB. Following

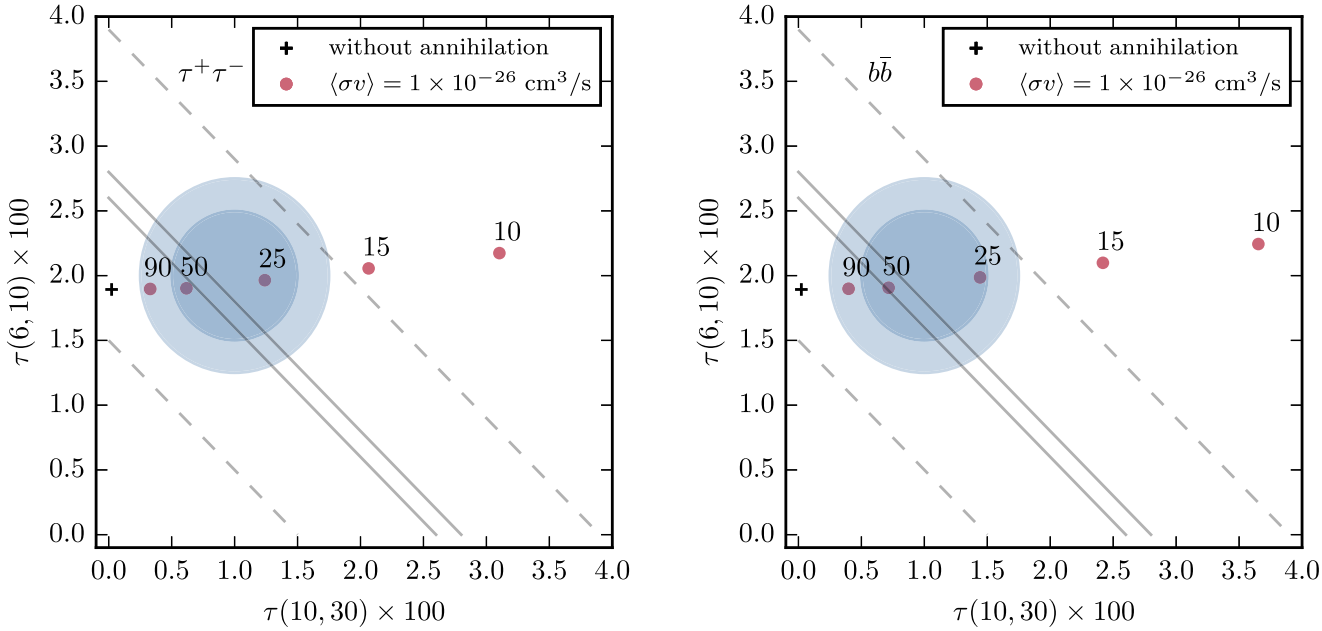

Figure 5. Constraints on the optical depth integrated over two redshift ranges: $z = 6$–10 and $z = 10$–30. The dashed and solid gray lines are contours of constant total optical depth, $\tau = 0.066 \pm 0.012$ (current precision, Planck Collaboration et al. 2016) and $\tau = 0.066 \pm 0.001$ (as expected with future 21 cm data, Liu et al. 2016b), respectively. The blue shaded regions are the estimated constraints from a principal component analysis of cosmic variance limited CMB polarization data (Mortonson & Hu 2008). The black cross denotes our fiducial reionization model, without any contribution from DM annihilation, while the red points denote the predictions including DM annihilating with a cross-section $\langle\sigma v\rangle = 1 \times 10^{-26}\,\mathrm{cm}^2$, for various values of the DM mass (in GeV) and for our *High* boost factor model. Results are shown for DM annihilating to $\tau^+\tau^-$ (left) and $b\bar{b}$ (right).

the method presented by Mortonson & Hu (2008), one can decompose τ into redshift bins, allowing us to separate the early effects of DM annihilation from the contribution from stars and quasars, which are localized at relatively lower redshifts (e.g., see Kuhlen & Faucher-Giguère 2012 for a wide parameter study). With this goal in mind, we adopt redshift bins of 6–10 and 10–30, and plot these results in Figure 5, along with the existing and projected constraints from CMB polarization measurements. We show the results for DM annihilating to $\tau^+\tau^-$ (left) and $b\bar{b}$ (right), with a cross-section of $10^{-26}\,\mathrm{cm}^3\,\mathrm{s}^{-1}$. Each numbered red point represents the prediction for a DM particle of a given mass, adopting our *High* boost factor model. The models with lower boost factor scale these figures along the x-axis, making the decomposition less constraining. Such a decomposition could plausibly be used to distinguish the effects of DM annihilation from astrophysical sources of reionization, and perhaps even provide an approximate measurement of the DM particle mass.

The decomposition constraints presented here are independent on the reionization model (Mortonson & Hu 2008). However, in our case the variation of the possible reionization histories is defined. Therefore, for a fixed family of models for annihilation and boosting factor, one can come up with a more constraining approach based on principal component analysis instead of just using two redshift bins.

5. DISCUSSION AND SUMMARY

Given the current state of observation and theory, it is not yet possible to use the reionization history of the universe to place strong constraints on annihilating DM. There are compelling reasons, however, to expect that this may change in the coming years. Uncertainties regarding the profiles, concentrations, and other features of low-mass DM halos and subhalos are likely to be reduced as simulations improve. In parallel, improvements in hydrodynamical simulations, combined with empirical input from *JWST* and 21 cm observations, will enable us to more accurately predict the contribution to reionization from stars and quasars. Finally, determinations of the universe's optical depth, τ, are expected to become much more accurate as CMB polarization and 21 cm measurements proceed. Ultimately, the universe's optical depth could be decomposed into redshift bins, allowing us to separate the early effects of DM annihilation from lower redshift sources of ionizing photons. Taken together, it appears plausible that the reionization history of the universe could, in the foreseeable future, provide a valuable and complementary probe of annihilating DM, allowing us to place constraints on the DM's mass, annihilation cross-section and channel, and even the minimum halo mass, as determined by the temperature of kinetic decoupling.

Last, we note that the heat produced through DM annihilation could also impact the evolution of the IGM. The temperature of the IGM and CMB decouple at redshift $z \sim 140$, after which the gas cools more quickly than radiation. Later, this gas is reheated during reionization by stars, although there are proposed mechanisms, which could preheat the IGM prior to this stage, including X-rays from high-mass X-ray binaries (Jeon et al. 2014) and supermassive black holes (Tanaka et al. 2012). The rising temperature of the IGM increases the filtering scale, reducing the clumping factor (Jeon et al. 2014), thus decreasing the recombination rate and speeding reionization. The complexity and interconnection of these effects can be reliably studied only in numerical simulations.

Fermilab is operated by Fermi Research Alliance, LLC, under Contract No. DE-AC02-07CH11359 with the United States Department of Energy. This work was also supported in part by the NSF grant AST-1211190.

REFERENCES

Anderhalden, D., & Diemand, J. 2013, JCAP, 4, 009
Angulo, R. E., Hahn, O., Ludlow, A., & Bonoli, S. 2016, arXiv:1604.03131
Becker, G. D., Bolton, J. S., Madau, P., et al. 2015, MNRAS, 447, 3402
Behroozi, P. S., Wechsler, R. H., & Conroy, C. 2013, ApJ, 770, 57
Belikov, A., & Hooper, D. 2009a, PhRvD, 80, 035007
Belikov, A. V., & Hooper, D. 2009b, PhRvD, 80, 035007
Bergström, L., Bringmann, T., Cholis, I., Hooper, D., & Weniger, C. 2013, PhRvL, 111, 171101
Chuzhoy, L. 2008, ApJL, 679, L65
Ciafaloni, P., Comelli, D., Riotto, A., et al. 2011, JCAP, 3, 19
Cirelli, M., Corcella, G., Hektor, A., et al. 2011, JCAP, 3, 051
Cirelli, M., Iocco, F., & Panci, P. 2009, JCAP, 10, 9
Cumberbatch, D. T., Lattanzi, M., & Silk, J. 2010, PhRvD, 82, 103508
Dalgarno, A., Yan, M., & Liu, W. 1999, ApJS, 125, 237
Diemand, J., Moore, B., & Stadel, J. 2005, Natur, 433, 389
Diemer, B., & Kravtsov, A. V. 2015, ApJ, 799, 108
Dvorkin, C., Blum, K., & Zaldarriaga, M. 2013, PhRvD, 87, 103522
Emberson, J. D., Kobayashi, T., & Alvarez, M. A. 2015, ApJ, 812, 9
Fermi-LAT Collaboration 2015, arXiv:1503.02641
Fialkov, A., Barkana, R., & Visbal, E. 2014, Natur, 506, 197
Furlanetto, S. R., Oh, S. P., & Pierpaoli, E. 2006, PhRvD, 74, 103502
Furlanetto, S. R., & Stoever, S. J. 2010, MNRAS, 404, 1869
Gnedin, N. Y. 2014, ApJ, 793, 29
Gnedin, N. Y., & Kaurov, A. A. 2014, ApJ, 793, 30
Green, A. M., Hofmann, S., & Schwarz, D. J. 2004, MNRAS, 353, L23
Hütsi, G., Hektor, A., & Raidal, M. 2009, A&A, 505, 999
Ishiyama, T. 2014, ApJ, 788, 27
Jeon, M., Pawlik, A. H., Bromm, V., & Milosavljevi, M. 2014, MNRAS, 440, 3778
Kaurov, A. A. 2016, ApJ, 824, 97
Kuhlen, M., & Faucher-Giguère, C.-A. 2012, MNRAS, 423, 862
Liu, A., Pritchard, J. R., Allison, R., et al. 2016b, PhRvD, 93, 043013
Liu, H., Slatyer, T. R., & Zavala, J. 2016a, PhRvD, 94, 063507
Lopez-Honorez, L., Mena, O., Palomares-Ruiz, S., & Vincent, A. C. 2013, JCAP, 7, 046
Madau, P., & Haardt, F. 2015, ApJ, 813, 8
Mao, Y.-Y., Williamson, M., & Wechsler, R. H. 2015, ApJ, 810, 21
Mapelli, M., Ferrara, A., & Pierpaoli, E. 2006, MNRAS, 369, 1719
Moline, A., Ibarra, A., & Palomares-Ruiz, S. 2015, JCAP, 6, 005
Mortonson, M. J., & Hu, W. 2008, ApJ, 672, 737
Naoz, S., Yoshida, N., & Gnedin, N. Y. 2013, ApJ, 763, 27
Natarajan, A., & Schwarz, D. J. 2009, PhRvD, 80, 043529
Navarro, J. F., Frenk, C. S., & White, S. D. M. 1997, ApJ, 490, 493
Planck Collaboration, Ade, P. A. R., Aghanim, N., et al. 2016, A&A, 594, A13
Poulin, V., Serpico, P. D., & Lesgourgues, J. 2015, JCAP, 12, 041
Press, W. H., & Schechter, P. 1974, ApJL, 187, 425
Profumo, S., Sigurdson, K., & Kamionkowski, M. 2006, PhRvL, 97, 031301
Ripamonti, E., Mapelli, M., & Ferrara, A. 2007a, MNRAS, 374, 1067
Ripamonti, E., Mapelli, M., & Ferrara, A. 2007b, MNRAS, 375, 1399
Sanchez-Conde, M. A., & Prada, F. 2014, MNRAS, 442, 2271
Shchekinov, Y. A., & Vasiliev, E. O. 2007, MNRAS, 379, 1003
Shull, J. M. 1979, ApJL, 234, 761
Shull, J. M., & van Steenberg, M. E. 1985, ApJL, 298, 268
Slatyer, T. R. 2016, PhRvD, 93, 023521
Slatyer, T. R., Padmanabhan, N., & Finkbeiner, D. P. 2009, PhRvD, 80, 043526
Tanaka, T., Perna, R., & Haiman, Z. 2012, MNRAS, 425, 2974
Tinker, J., Kravtsov, A. V., Klypin, A., et al. 2008, AJ, 688, 709
Valdés, M., Evoli, C., & Ferrara, A. 2010, MNRAS, 404, 1569
Valdés, M., Ferrara, A., Mapelli, M., & Ripamonti, E. 2007, MNRAS, 377, 245
Zahn, O., Reichardt, C. L., Shaw, L., et al. 2012, ApJ, 756, 65
Zavala, J., & Afshordi, N. 2016, MNRAS, 457, 986